Title

Characterizing the neural circuitry associated with configural threat learning

Authors

Stout, Daniel M
Glenn, Daniel E
Acheson, Dean T
et al.

Publication Date

2019-09-01

DOI

10.1016/j.brainres.2019.06.003

Peer reviewed

Published in final edited form as:

Brain Res. 2019 September 15; 1719: 225–234. doi:10.1016/j.brainres.2019.06.003.

Characterizing the Neural Circuitry Associated with Configural Threat Learning

Daniel M. Stout[1,2,*], **Daniel E. Glenn**[3], **Dean T. Acheson**[1,2], **Alan N. Simmons**[1,2,†], **Victoria B. Risbrough**[1,2,†]

[1]Center of Excellence for Stress and Mental Health, VA San Diego Healthcare System, San Diego, CA 92161 USA

[2]Department of Psychiatry, University of California San Diego, San Diego, CA 92093 USA

[3]Semel Institute for Neuroscience and Human Behavior, University of California Los Angeles, Los Angeles, CA 90095 USA

Abstract

Contextual threat learning is often associated with two processes: elemental and configural learning. Few studies have examined configural learning where subjects form a representation of the threat-related context as a gestalt whole from the individual features in the environment. The goal of the current study was to compare and contrast neural circuitry recruited by variation in demands placed on configural threat encoding. Subjects (N=25) completed a configural threat learning task, where we manipulated the amount of configural encoding required to learn the threat association (low demand: changes to a discrete element of the context; and high demand: rearrangement of elements). US expectancy ratings, skin conductance responses (SCR), and functional magnetic resonance imaging (fMRI) were collected. Subjects successfully learned the configural threat association as measured by US expectancy ratings, SCR, and BOLD activity. Hippocampal and amygdala region of interest analyses indicated differential configural threat learning and predicted SCR measures of learning. Furthermore, whole brain analyses identified four circuits that were impacted by the amount of differential configural encoding required, but none correlated with SCR. These results set the stage for a more detailed understanding of how configural threat learning is instantiated in the brain—an important mechanism associated with PTSD and other fear-related disorders.

[*]**Address correspondence to:** Daniel M. Stout, Ph.D. (dastout@ucsd.edu), Center of Excellence for Stress and Mental Health, VA San Diego Healthcare System, Department of Psychiatry, University of California San Diego, 3350 La Jolla Village Drive, San Diego, CA 92161, Phone: 858-642-1253.

[†]Both authors contributed equally to this work

CONFLICT OF INTEREST STATEMENT

The authors declare that they have no competing or conflicts of interests.

DATA AVAILABILITY

Data and code will be made available upon request.

Keywords

Contextual fear; Configural learning; Threat processing; Fear conditioning; fMRI

1. INTRODUCTION

Posttraumatic stress disorder (PTSD) and fear-related disorders are associated with deficits in correctly interpreting threat and safety cues, in particular in using contextual information to modulate defensive and affective responses (Acheson et al., 2012; Glotzbach-Schoon et al., 2013; Ledoux and Daw, 2018; Liberzon and Abelson, 2016). Environmental context determines whether environmental cues are threat-related (e.g., road-side object on a desert road while during a convoy in a combat zone) or safe (e.g., road-side object on the freeway on your commute to work) (Urcelay and Miller, 2014). Contexts are comprised of the multimodal "background" features (e.g., spatial, temporal, internal, and cognitive) that provide relevance to an object (Maren et al., 2013). To better inform diagnostic and treatment decisions for PTSD, there is a need to first understand the neural mechanisms associated with the different components of contextual threat learning.

Contextual threat learning reflects, in part, two processes: elemental and configural learning (Rudy, Huff, & Matus-Amat, 2004; Rudy, 2009). Elemental encoding involves acquiring the context representation via independent elements or features within the environment (Rudy et al., 2004; Urcelay and Miller, 2014). In contrast, configural threat learning involves forming a representation of the threat-related context as a gestalt whole from the individual features or elements (e.g., the tone, the shock electrode leads, the furniture in the laboratory, the background sounds of the building, any smells; Rudy, 2009). The relationship between elemental and configural processes over threat learning governs whether a defensive response is triggered by a single element or by the entire context (Maren et al., 2013). Context is a broad, multifaceted construct, so it is perhaps unsurprising that investigators have used varying methods to investigate human contextual threat (Glenn et al., 2018). The broad definition of context has led to methodological challenges for dissociating the neural activity between configural and elemental threat learning.

Previous human neuroimaging investigations of contextual threat learning studies have primarily measured the neural activity associated with distinguishing between simple backgrounds (e.g., different colors, background pictures) to learn when a threatening stimulus would be presented depending on the background scene (Lang et al., 2009; Pohlack et al., 2012). Studies using such paradigms have found a broad set of neural activation associated with differential contextual threat learning, including the amygdala, hippocampus, medial prefrontal cortex, anterior cingulate cortex, dorsolateral- and ventrolateral prefrontal cortices, and the insula (Alvarez et al., 2008; Andreatta et al., 2015; Marschner et al., 2008). Although much has been learned about the neural circuitry associated with contextual threat learning using these paradigms, differentiating backgrounds can be solved by manipulating a single feature or element. Thus, the role that configural encoding plays in threat learning remains poorly understood (Glenn et al., 2018).

Animal studies indicate that configural threat learning is hippocampal-dependent (Fanselow, 2000; Monti et al., 2014; Rudy, 2009). The two human neuroimaging studies that have examined configural threat learning have supported the important role that the hippocampus plays in configural threat encoding (Baeuchl et al., 2015; Stout et al., 2018). Yet, configural processing also places demands on other circuits important for spatial relational-processing and higher-level cognition (Brodt et al., 2016; Robin et al., 2015) and fear conditioning (Glenn et al., 2018). Moreover, distinguishing between high and low configural encoding demands within the same task has not been tested and will be critical to separate the basic fear learning circuitry from configural threat encoding (Baeuchl et al., 2015; Stout et al., 2018). To this end, the aim of the current study was to characterize the neural circuitry associated with varying demands placed on configural threat learning.

Subjects completed a configural threat learning task (Stout et al., 2018) while undergoing functional magnetic resonance imaging (fMRI)(See Figure 1). Specifically, subjects were required to learn that one specific configuration was associated with an aversive air-puff to the throat (configural CS+; CON+). In other conditions they viewed the same pieces of furniture in the same room but the furniture items (or elements) were shuffled into a different arrangement (configural CS-; CON-) or were in the same arrangement as CON+ but a single piece of furniture was replaced with a new one (configural CS- element replaced; CON-ER). Two more conditions were presented which consisted of either a new set of furniture arranged in a room (new context CS-; CXT-) or a similar condition where one item (or element) from CON+ was added to the three items from CXT- (new context CS- element added; CXT-EA) (See Table 1 and Methods section for more details). This approach allowed us to compare the neural circuitry associated with varying levels of configural encoding demands. We hypothesized that compared to the CON+ condition, low configural demands (e.g., based upon a changing background) would recruit lower-level sensory circuits more so than configural-based threat learning. We also hypothesized that frontoparietal regions would be more prominent when greater demands were placed on configural threat learning compared to learning that required less configural processing (i.e., elemental learning). We measured skin conductance response to cues as well as self-reported US expectancy as operational measures of threat response.

2. RESULTS

2.1 US expectancy

As shown in Figure 2a, subjects learned to differentiate the configural threat condition (CON+) from the other conditions, however there was a graded expectancy for the US to CS- trial types depending on the level of configural demand. The main effects of CS Type was significant ($p < 1.5 \times 10^{-9}$). US expectancies were higher for CON+ than all other conditions (*ps* <.001; FDR adjusted). US expectancies were significantly higher for CON-ER (CON+ room with one element replaced) than CON- (same room as CON+ with elements rearranged), CXT-EA (new room with one element from CON+), and CXT- (new room and elements) (*ps* <.008; FDR adjusted).

2.2 SCR

The main effect of CS Type and Block were significant (*F*s>5.38, *ps*<.002). As shown in Figure 2b, SCR for CON+ was significantly greater than the other four conditions (*ps*<.041; FDR adjusted), whereas there were no differences between the other conditions *ps*>.87).

2.3 fMRI: Hippocampus and amygdala

We computed a CS Type voxel-wise linear mixed-effects model (3dLME; Chen et al., 2013) for both the hippocampus and amygdala regions of interest (ROIs). As shown in Figure 3, we observed three clusters in the hippocampus that significantly differentiated the five conditions. Activity in the left anterior hippocampus (*X*= −24, *Y*= −15 , *Z*= −14, 7 voxels, *peak F*-value= 5.70), was greater for CON+ compared to trials with the same elements rearranged (CON-) or in the same configuration with one element replaced (CON-ER)(*p*s <.02; FDR adjusted) but was not different from trials using a totally different room (CXT-) or different room with only one element from CON+ (CXT-EA; *p*s > .39; FDR adjusted; Figure 3a). In the left posterior hippocampus however (*X*= −28, *Y*= −32, *Z*= −10, 7 voxels, *peak F*-value= 5.46; Figure 3b), showed no activity difference between CON+ and CON- (*p* =.23; FDR adjusted), but was higher than CON-ER and CXT-EA conditions (*p*s < .01; FDR adjusted) and marginally higher than CXT- (*p*=.06; FDR adjusted). Activity in the right posterior hippocampus (*X*= 32, *Y*= −29, *Z*= −10, 4 voxels, *peak F*-value= 5.45; Figure 3c) was associated with greater activity for CON+ than the other conditions (*p*s <.03; FDR adjusted) except for CXT- (*p* = .40; FDR adjusted). Finally, we also observed a cluster in the left amygdala that displayed significant condition differences (*X*= −21, *Y*= −1, *Z*= −24, 23 voxels, *peak F*-value= 8.74; Figure 4). Amygdala activity for CON+ was significantly greater than the other conditions (*p*s < .05; FDR adjusted) except for the CXT- condition (*p* = .10; FDR adjusted).

2.4 fMRI: Whole-brain

The results of the whole-brain analysis revealed a broad set of neural regions that differentiated the five CS types (See Figure 5). Among these regions were the dlPFC, dorsomedial PFC, bilateral posterior parietal cortex (PPC), periaqueductal grey area (PAG), anterior insula (aINS), caudate, and thalamus. See Table 2 for a list of all of clusters observed and the PSC for each condition.

To reduce the number of post-hoc comparisons, we performed a *k*-means cluster analysis to identify clusters of regions that have similar patterns in neural activity and may be sensitive to particular condition differences. As Figure 6a–b shows, a four-cluster model was determined to produce the best distribution of the neural regions (*k*=4; gap=0.196, *SE*=0.095) versus a 2, 3, or 5 cluster model (gaps <.190, *SE*s >.099; See Supplementary Table 1 and Supplementary Figure 2). The relationship between the *k*=4 model clusters and the individual regions within each cluster are reported in the Supplementary Materials (Supplementary Figures 3–6).

Cluster 1 consisted of the post cingulate gyrus, posterior insula (pINS), paracentral gyrus, and the supramarginal gyrus (see Supplementary Figure 3). As shown in Figure 6c, neural activity from regions in Cluster 1 was significantly higher for CON+ than the other four

conditions (*ps* <.01, FDR adjusted). Neural activity between the safe conditions did not differ (*p*s>.14).

Cluster 2 consisted of the anterior insula (aINS), the right and left caudate, dorsolateral prefrontal cortex (dlPFC), dorsomedial PFC (dmPFC), and the periaqueductal grey area (PAG) (see Supplementary Figure 4). Neural activity in this cluster was significantly greater in all of the Room A conditions (i.e. the high configural demand conditions, CON+, CON-, and CON-ER) than Room B conditions (i.e. low configural demand conditions, CXT-, CXT-ER), *ps*<.003 (FDR adjusted). Neural activity across the Room A conditions did not differ from each other, *ps*>.37 (Figure 6d).

Cluster 3 consisted of the left and right posterior parietal cortex (see Supplementary Figure 5). Neural activity in these regions were greater in the CON- and CON-ER conditions than in the other three conditions, *ps*<.05 (FDR adjusted; Figure 6e). CON+ and the different context conditions were not significantly different from each other, *ps*>.27 (FDR adjusted).

As shown in Figure 6f, Cluster 4 consisted of the left and right thalamus and the supplemental motor area (SMA) (see Supplementary Figure 6). Neural activity in these regions were significantly higher for the CON+ than the other four conditions (*p*s <.001; FDR adjusted). This result is supported by significant differences between the configural conditions (CON-ER & CON-) and the different context conditions (CXT-EA & CXT-), *ps* < .02 (FDR adjusted).

Although our goal of the cluster analysis was to facilitate interpretation of the whole-brain analysis, we conducted a second *k*-means analysis that included the three hippocampus regions and the amygdala region that were identified via the ROI analysis. Results of this analysis are reported in the Supplementary Figure 7.

2.5 SCR & brain correlations

Differential CON+ and CON- SCR correlated with the differential CON+ and CON- neural activity in the left posterior hippocampus, $r(22)=.50$, $p=.012$ (uncorrected). A similar pattern was observed for the CON+ > CON-ER and CON+>CXT-EA difference scores (*ps*<.041; uncorrected) but not for CON+>CXT- ($p=0.2$; uncorrected). Differential CON+ and CON- SCR also correlated with the differential CON+ and CON- neural activity in the right posterior hippocampus, $r(22)=.41$, $p=.046$ (uncorrected) and the amygdala, $r(22)=.44$, $p=.034$ (uncorrected). See Supplementary Figure 8 for scatter plots depicting the significant relationships. No other neural region or cluster correlated with SCR (*ps* > .06; uncorrected).

3. DISCUSSION

The goal of the current investigation was to characterize the neural circuitry associated with configural threat learning. Subjects completed a configural threat learning task where configural processing demands were manipulated via the arrangement of furniture within the same background or through discriminating changed elements in the same or different background. Results of the current study show that subjects successfully discriminated between the threat and safety configurations as measured by US expectancy ratings, SCR,

and BOLD activity. Supporting previous investigations, we observed that the hippocampus and the amygdala play key roles in configural threat learning and activity in these regions predicted SCR to theat. Furthermore, using *k*-means clustering on the neural regions identified in a whole-brain analysis, we identified four circuits that showed differential neural activity depending on the configural demands necessary to learn threat from safety. Collectively, these results confirmed that configural threat learning requires the coordination of several distinct and overlapping neural circuits, with each circuit contributing to a facet of configural processing — a key process involved in contextual threat learning.

Our findings support the role of the hippocampus and amygdala in configural threat learning (Maren et al., 2013; Rudy, 2009). Hierarchical representations of a context are formed via the hippocampus by linking single environmental features into a single contextual configuration or representation (Fanselow, 2000; Maddox et al., 2019; Rudy et al., 2004). Configural threat representations in the hippocampus send downstream output-signals directly to the basolateral nucleus of the amygdala (BLA) to initiate a defensive response (Knapska et al., 2012; Maren et al., 2013). Consistent with this, disrupting hippocampal activity via lesion and optogenetic manipulations is associated with reduced configural threat learning and contextual memory retrieval (Anagnostaras et al., 2001; Corcoran and Maren, 2001; Kheirbek et al., 2013). Moreover, increased bidirectional theta oscillations between the hippocampus and the amygdala are associated with successful emotional pattern separation in humans (Zheng et al., 2019). Neuroimaging studies consistently find increased hippocampal and amygdala activation to threat-related configurations (Baeuchl et al., 2015; Stout et al., 2018) and threatening contexts (Alvarez et al., 2008; Marschner et al., 2008). Here we show that activity in the left posterior hippocampus was particularly important for configural encoding. We observed significantly greater activity for the conditions that required the highest configural encoding demands to differentiate threat from safety (i.e., CON+ and CON-). We designed the CON- condition to maximize configural encoding by maintaining feature-identical elements across both conditions. To differentiate CON+ from CON-, learning of the higher-order spatial-relationship between the elements is necessary (Glenn et al., 2017). In sum, the results of our study demonstrate that the posterior hippocampus is central to forming configural representations associated with threats.

Whole brain analyses revealed that configural threat learning is characterized by a set of neural circuits that subserve distinct but overlapping functional roles. We observed three circuits that significantly differentiated the configural conditions from elemental-background context conditions (Clusters 2–4). Cluster 2 was comprised of neural regions that are implicated in anticipatory threat processing (Brinkmann et al., 2017; Craig, 2009; Drabant et al., 2011; Grupe et al., 2013; Somerville et al., 2013). This circuit consisted of the caudate, dorsolateral prefrontal cortex (dlPFC), dorsomedial prefrontal cortex (dmPFC), anterior insula (aINS), and the periaqueductal gray area (PAG). Thus, the observation that these regions were significantly recruited for the conditions that placed greater demands on configural processing, regardless of threat level, likely indicates the subjects were responding to rooms that signal the potential of receiving the US and not specific to configural processing per se—circuitry associated with broader fear learning and conditioning (Glenn et al., 2018).

For Cluster 3, we observed that the left and right parietal cortex regions clustered together. Neural activity in these regions was higher for the two configural conditions that were not associated with the US (CON-ER & CON-) than the CON+ and the two different context conditions (CXT- & CXT-EA). The posterior parietal cortex (PPC) is part of the dorsal attention network and aids episodic memory (Cabeza et al., 2008). PPC facilitates representation of the spatial relationship between objects and the formation of spatial memories (Baumann and Mattingley, 2014; Brodt et al., 2016). Lesions to the PPC result in the impairment of spatial location memory (Saj et al., 2018) and functional connectivity between the PPC and the hippocampus is increased during spatial memory tasks (Robin et al., 2015). The results observed in our study suggest that increased PPC activity for the safe configural conditions may be due to the attentional demands required for forming hierarchical representations of spatially-related items— a requisite for configural encoding in the current investigation.

The neural regions that comprised Cluster 4 consisted of the thalamus and the SMA. The thalamus is highly connected to subcortical and cortical brain networks including the SMA (Fang et al., 2006; O'Muircheartaigh et al., 2015), making it well positioned to influence cognitive and affective processing (Schmitt et al., 2017; Arend et al., 2015). Furthermore, thalamic activity is associated with responding to changes in processing demands depending on contextual information (Rikhye et al., 2018). The SMA supports motor planning and predicting the consequences of movement (Makoshi et al., 2011). Furthermore, the SMA is integral to executing regulation strategies to resolve emotional conflict (Deng et al., 2014) and is associated with emotion regulation and treatment success in individuals diagnosed with PTSD (MacNamara et al., 2016). The pattern observed in the current study could reflect the coordination of neural resources for the implementation of emotion regulation strategies when expecting potential threats.

Cluster 1 consisted of the post cingulate gyrus, posterior insula (pINS), paracentral gyrus, and the supramarginal gyrus. Activity in this cluster was significantly greater for the CON+ compared to the other four conditions. The pINS is important for interoception of aversive stimulation (Khalsa et al., 2009; Segerdahl et al., 2015) and the posterior cingulate gyrus is associated with physiological responding (Vogt, 2005). These results suggest that this cluster forms a circuit involved in interoceptive awareness and responding to the CON+ - US association. It is notable that the magnitude of average PSC for all of the non-CON+ conditions were significantly higher for Clusters 2–4 compared to those same conditions in Cluster 1, indicating that Clusters 2–4 were more robustly recruited in our paradigm. In a second clustering analysis (see Supplementary Figure 7), we observed that the hippocampus and amygdala regions were assigned to this cluster, indicating that these regions contribute to learning the threat contingency and physiological responding. The remaining regions clustered together to form a circuit that differentiated the Room A conditions from the Room B conditions, indicating responding to potential or contextual threats.

Our results show that varying levels of configural threat learning have unique and overlapping neural circuits (Glenn et al., 2017; Rudy et al., 2004; Stout et al., 2018). We show that high and moderate configural threat encoding demands require neural circuits that subserves spatial-relational processes (e.g. parietal cortex, thalamus); whereas low

configural demands requiring the differentiation between backgrounds recruits neural circuits that are commonly observed in anticipating potential threats and threat conditioning (e.g. aINS, pINS, caudate, PAG) (Fullana et al., 2016; Grupe & Nitschke, 2013). Importantly, we show that both the hippocampus and amygdala play critical roles in configural threat learning and both predicted SCR measures of learning. It should be noted that the circuits identified through the whole-brain analyses were not significantly associated with the SCR measures. One interpretation is that these circuits play a computational or support role regarding the different threat predictors (e.g., elements versus configuration, context changes) and relay this information to output circuits associated with defensive responding and fear expression (i.e., the hippocampus and amygdala).

From a translational perspective, our findings have important implications for trauma-related (e.g., PTSD) and fear-related disorders (e.g., Panic Disorder, Specific Phobias, etc.). Impairment in contextual threat learning is an important phenotype associated with PTSD (Joshi et al., 2019; Liberzon and Abelson, 2016; Maddox et al., 2019). We have previously hypothesized that hippocampal-based configural learning processes may be most disrupted in PTSD populations, allowing for the dominance of amygdala-driven elemental strategies (Acheson et al. 2012). A failure to utilize configural processing may result in defensive responding to single elements in inappropriate contexts (e.g., fear response to a similar smell or sound as experienced during the trauma in a completely different environment). Yet, few human neuroimaging studies have investigated configural threat learning in PTSD populations. Therefore, more work is needed to examine which aspect of contextual threat learning is impaired in PTSD (Steiger et al., 2015).

There are limitations that need to be addressed. First, there were an unequal number of trials of Room A (CON+, CON-, CON-ER; 28 total trials) and Room B (CXT- and CXT-EA; 16 total trials). This may have unintendedly produced a novelty effect for the Room B conditions, for which the amygdala and hippocampus play a critical role (Pedersen et al., 2017b, 2017a). Second, we did not counter-balance the assignment of the CON+ to the two different rooms. Thus, generalizability of our findings needs to be tested in future studies. Third, we did not directly compare neural activity associated with configural threat encoding with neural activity associated with threat learning using a single cue (e.g., elemental learning). However, to solve CON+ versus CON-, configural encoding is necessary and using an elemental approach would lead to a failure to differentiate these conditions. Therefore, the comparison between these two conditions would be an accurate test of configural learning. In addition, our results broadly replicate our prior work showing that hippocampal activity and posterior parietal BOLD activity is particularly relevant for configural threat learning and less so for elementally-based threat learning (Stout et al., 2018). An important challenge for future work will be to test configural threat memory recall performance at later time-points (e.g., 24 hours later). This extension would be helpful for identifying the neural circuitry associated with how threat-related memory encoding strategies influence subsequent defensive responses, particularly whether presentation of a single element or the full configuration is required to elicit a response—an important implication for PTSD (Acheson et al., 2012; Liberzon and Abelson, 2016).

In conclusion, the current study provides new evidence for the circuits that underlie configural threat learning. We show that the hippocampus and amygdala are strong candidates for driving configural threat encoding. Beyond these two canonical regions, we show that there are multiple circuits operating depending on the extent to which configural processing demands are required. Circuits associated with fear expression and sensory responding (e.g., PAG, insula, PFC, caudate, and the thalamus) are important if a threat context can be learned via low configural demands. When there is an additional requirement to encode a configuration of several elements to determine the threat-level, PPC recruitment is enhanced. Identifying the neural mechanisms associated with configural threat learning is important for delineating how contextual threats are learned. Importantly, these results may provide key insights into the etiology and maintenance of neuropsychiatric disorders associated with a dysfunction in managing contextual encoding processes related to threat learning and expression.

4. EXPERIMENTAL PROCEDURE

4.1 Participants

A total of 25 subjects (mean age=30.08, *SD*=11.30, range= 18–55; 14 female) from the San Diego area completed the contextual threat learning task while undergoing fMRI. The majority of subjects were right-handed (n=24) as measured by a single self-reported question. Based on our experience using a similar task, we have achieved large effect sizes using a similar sample size (Stout et al., 2018). Informed consent was obtained from all subjects prior to participating and were monetarily compensated. Ethical considerations and study procedures were approved by the institutional review board of the University of California San Diego.

4.2 Configural threat acquisition task

The configural threat acquisition task was adapted from the paradigm detailed in Stout et al. (2018). During this task (see Figure 1 and Table 1), subjects viewed computer-generated pictures of four furniture items in one of two room (7.5 seconds). In this task, a specific arrangement of furniture items in a room was paired with an unconditioned stimulus (configural CS+; CON+). The unconditioned stimulus (250 psi air puff) was delivered via a plastic tube positioned 2.5 cm from the center of the throat. Along with the CON+, subjects completed four other conditions that required varying configural encoding demands. 1) Subjects completed a condition that contained the same four pieces of furniture in the same room as CON+, but the furniture items were shuffled into a different arrangement and was not paired with the air-puff (configural CS-; CON-). To differentiate the CON+ from the CON-, subjects would be required to encode a hierarchical representation of the spatial relationships between each piece of furniture (a high configural demand). 2) Subjects completed another condition that was identical to the CON+ configuration except that one piece of furniture was replaced with a new piece and the US was not delivered (configural CS- element replaced; CON-ER). To differentiate the CON+ from CON-ER trials, a moderate level of configural encoding would be required. Two conditions with low levels of configural encoding demands were included. These consisted of 1) a new room with four new pieces of furniture (new context CS-; CXT-) that would require low to no configural

encoding demands to differentiate it from CON+, and 2) a similar condition as CXT- but one piece of furniture from CON+ was added (new context CS- element added; CXT-EA), which would require low levels of configural demands to differentiate it from the CON+ condition.

An inter-trial interval (ITI) of 7.5 to 10.5 seconds separated the trials. The US co-terminated with CON+ on 100% (12/12) of trials, but never with the other four conditions (8 trials each) or during the ITI. To prevent front- or back-loading CON+ trials in a pure randomized trial design (Lonsdorf et al., 2017), trials were sequenced in one of two fixed orders, where each order had the trials presented in a pseudo-random order such that the CON+ did not appear on more than two consecutive orders. There was a total of 44 trials.

4.3 US expectancy analysis

US expectancy awareness was measured during each trial using the button box to report whether or not they expected the air puff. Subjects responded, with their dominant hand, with a “1” if they expected the air puff, “2” if they were unsure, and “3” if they did not expect the air puff. The scale remained on the screen for the entire 7.5 second duration of each event. If no response was made, a no response was recorded. However, all subjects made a response during the interval. Expectancy responses were then re-coded to 1, 0, −1 for analyses. We then computed a Cue Type repeated-measures analysis of variance on the expectancy ratings. Results for Cue Type X Block analysis is reported in Supplementary Figure 1. Corrections for multiple post-hoc comparisons were conducted using the false discovery rate (FDR $q < .05$) and the adjusted p-values are reported (Benjamini and Hochberg, 1995).

4.4 SCR measurement and analysis

SCR was measured using a Biopac MP150 unit running Acqknowledge 4.3.1 software (Biopac Systems Inc., Goleta, CA) connected to an EDA100C-MRI amplifier with a 5 μS/V gain and a 10.0-Hz low-pass filter. Skin conductance signals were acquired using two Ag/AgCl 11mm electrodes (EL509) filled with isotonic recording electrode gel (GEL101) and placed on the thenar and hypothenar eminence of the non-dominant hand so that they could use their dominant hand for task responding. Prior to electrode placement, the skin was lightly abraded. Next, verification of SCR responding was conducted by having subjects hold their breath for 10 seconds or make a fist in the opposite hand where the electrodes were placed. All subjects were observed to have a SCR during this procedure. During the experiment skin conductance Response (SCR) was continuously recorded to the nearest microsiemens (μS) during each trial and ITI, with raw SCR data transformed through mean value smoothing. Due to equipment malfunction, SCR for one subject was not recorded, leaving a total of 24 subjects with usable SCR. All subjects had a SCR response as defined as average minimum > 0.1 μS (0.01 per Boucsein et al., 2012; Pineles et al., 2016) (average minimum peak=4.41, SD=1.26, largest minimum response=2.58). Similar to our prior work (Stout et al., 2018) and by others (Orr et al., 2000), a peak response within a post-stimulus onset window was used to estimate SCR magnitude. The benefit of this approach is that it makes no assumptions about when the peak occurs within the time window and therefore limits underestimating an SCR if the first response peak is used (Pineles et al., 2009). Peak responses were calculated as the difference between the mean SCR within the 2-second

period prior to stimulus onset subtracted from the maximum (peak) SCR within a 1–6 second onset latency post-stimulus onset window. SCR magnitudes were standardized using a with-in subjects *Z*-score ($SCR_{trial\ n} - SCR_{mean} / SCR_{SD}$), where the SCR_{mean} and SCR_{SD} were estimated across all trials and conditions. Trials with outliers (± 3 standard deviations from the mean) were transformed via within-subject winsorizing (Wilcox and Keselman, 2003). We observed three subjects showing a mean fear response below zero for the CON+ (after subtracting baseline). These subjects could be classified as "non-responders." However, we include these subjects in our SCR analyses to reduce creating a performance-based exclusion bias and because these subjects may represent an important end of the fear learning spectrum (Lonsdorf et al., 2017; Lonsdorf and Merz, 2017). Post-hoc pairwise comparisons were FDR α-adjusted ($q<.05$) when necessary. For individual trial-level data, please see the Supplementary Materials.

4.5 MRI acquisition and preprocessing

MRI data were acquired using a 3T GE CXK4 scanner, which was equipped with 8-channel headcoil. High resolution T_1-weighted anatomical images were acquired using a spoiled gradient recalled echo sequence (FOV=25cm; matrix=256 × 256; 176 sagittal slices; 1mm thickness; TR=8ms; TE=4ms; flip angle=12°). Functional data were acquired using a T_2*-weighted echo planar image (EPI) sequence (matrix=64 × 64; 30 axial slices; in-plane resolution=3.75 × 3.75 × 4; gap=1.0mm; TR=1.5s; TE=30; flip-angle=80°). Prior to scanning, we included additional padding around the subject's head to reduce movement-related artifacts.

Preprocessing was similar to steps detailed in Stout et al. (2018). Imaging analysis was conducted using FSL (Jenkinson et al., 2012) and AFNI (Cox, 1996). Identification of excessive motion artifact was conducted using independent component analysis (ICA) with FSL Melodic which robustly identifies noise corresponding to movement (Beckmann and Smith, 2004). Motion artifact-related activity was then removed (Kelly et al., 2010). The motion-reduced images were then entered into standard preprocessing using AFNI. The first 2 volumes of each EPI scan were removed, and the remaining volumes were despiked, slice time corrected, volume registered for residual motion-related artifact where volumes were censored using a motion derivative cutoff of 0.3 (mean motion= 0.056 after ICA, after censoring an average of 98.91 volumes were retained), and spatially normalized into MNI standard space. Datasets were visually inspected for quality assurance. EPI data were spatially smoothed (6-mm FWHM) and converted to percent signal change.

The five condition trials (CON+, CON-, CON-ER, CXT-, CXT-ER) were modeled separately using a 7.5 second boxcar function and convolved with the hemodynamic response. Drift (linear and quadratic), motion (L/R, A/P, S/I, roll, pitch, yaw, and derivatives), censored time-points, and US onset were included as regressors of no interest.

4.6 Hippocampus and amygdala region of interest (ROI) analyses

The hippocampus and amygdala are important regions implicated in configural threat learning (Acheson et al., 2012; Glenn et al., 2018). To this end, we computed a Cue-Type repeated-measures linear mixed-effects model (*3dLME*; Chen et al., 2013) for both the

hippocampus and the amygdala. Using similar procedures to our prior work (Stout et al., 2018), we defined the left and right hippocampus and amygdala ROIs using from the Harvard-Oxford probabilistic atlas. These analyses were thresholded (p<.005) and small volume corrected (SVC; α < .05) using AFNI's *ClustSim* (10,000 simulations) within the volume of the hippocampus ROIs (cluster-size >4 voxels) and amygdala (cluster-size > 3 voxels) with the spatial auto-correlation function (*-acf*) to account for the non-Gaussian noise distribution (Cox et al., 2017). To examine condition differences, we extracted mean BOLD percent signal change (PSC) from observed hippocampal and amygdala clusters and entered them into SPSS (Version 25). Corrections for multiple comparisons were conducted using False Discovery Rate (FDR, q< .05) (Benjamini and Hochberg, 1995).

4.7 Whole brain analyses

To characterize configural threat learning beyond the hippocampus and amygdala, we computed an identical *3dLME* at the whole-brain. Results were voxel-level thresholded (p<.001) and cluster corrected (α<.05; cluster-size > 20 voxels) for multiple comparisons using *AFNI's 3dClustSim* with *-acf* (10,000 simulations). We extracted mean PSC from each significant region for each of the five conditions and submitted them to further analyses to test condition differences (see section 4.8 below).

4.8 Clustering analyses

Rather than selecting one or two regions from the whole-brain analysis to further explore the condition differences and rather than examining the condition differences for each region identified (n regions=15), we used a clustering approach. The goals of this analysis were to: 1) combine regions identified in the whole-brain analysis that displayed a similar pattern in differentiating conditions, and 2) reduce the number of post-hoc analyses to the number of clusters identified instead of the entire set of regions. Specifically, we computed a *k*-means clustering analysis using the group level mean PSC extracted from each region for each condition identified in the LME. *K*-means clustering is an unsupervised clustering algorithm that separates data into k clusters by selecting k initial cluster centers and then assigns each data point to their closest centroid. Then through an iterative process, assigns and updates each cluster's center until the within-cluster sum of squares is minimized (Kaufamn and Rousseeuw, 2008). In sum, the benefits of this analysis are (1) the identification of circuits that show similar patterns of activity in regard to differentiating conditions and (2) utilizing as much data as possible instead of restricting interpretation to an arbitrary selected region. Although we focused this *k*-means to identify broader circuits beyond the hippocampus and amygdala, we computed a second *k*-means analysis including the three hippocampal and the one amygdala region (see Supplementary Figure 7).

The *k*-means clustering analysis was performed in *R* using the '*cluster*' and '*factoextra*' packages. The input data set consisted of group-level PSC and was organized such that rows were regions identified from the whole-brain LME (n=15 regions) and columns were condition (n=5 conditions). Prior to analysis, the data were scaled to have a mean of zero and a standard-deviation of 1. We then performed *k*-means with Euclidean distance to cluster the pattern of neural regions. To determine the optimal number of clusters, we used the gap statistic. The gap statistic compares the total within-cluster sum of squares variation

for different values of *k* with their expected values from a null reference dataset created via Monte Carlo simulation (500 simulations) (Tibshirani et al., 2002). Higher gap scores denote greater difference from the null hypothesis (i.e., no observed clustering). The optimal cluster-size chosen is the smallest *k* with the highest gap statistic such that its value is not more than 1 standard error away from the first local maximum.

After we identified the clusters, we averaged the mean PSC from each region together within the respective cluster to form a single value representing that cluster. Cluster PSC was computed for each condition separately, allowing us to test pair-wise condition differences within the cluster. Corrections for multiple comparisons were conducted using FDR ($q < .05$).

4.9 SCR-brain relationships

To examine the relationship between configural threat learning and neural activity, we correlated BOLD response from the hippocampus, amygdala, and whole-brain network clusters with SCR. We first calculated four difference scores that corresponded to the difference between CON+ and the other four conditions: 1) CON+ > CON-ER, 2) CON +>CON-, 3) CON+>CXT-EA, and 4) CON+ > CXT-. These difference scores were computed for both SCR and neural regions. SCR difference scores were then separately correlated with neural region difference scores (Pearson 2-tailed). High scores indicate successful configural threat learning.

Supplementary Material

Refer to Web version on PubMed Central for supplementary material.

ACKNOWLEGEMENTS

This work was supported by the Center of Excellence for Stress and Mental Health at the VA San Diego and VA Merit Awards to VBR (IO1-BX002558) and ANS (I01-CX000292 & I01-CX000715). Writing of this manuscript was partially supported by the Office of Academic Affiliations, Advanced Fellowship Program in Mental Illness Research and Treatment, Department of Veterans Affairs (DMS).

REFERENCES

Acheson DT, Gresack JE, Risbrough VB, 2012 Hippocampal dysfunction effects on context memory: Possible etiology for posttraumatic stress disorder. Neuropharmacology 62, 674–685. [PubMed: 21596050]

Alvarez RP, Biggs A, Chen G, Pine DS, Grillon C, 2008 Contextual Fear Conditioning in Humans: Cortical-Hippocampal and Amygdala Contributions. J. Neurosci 28, 6211–6219. 10.1523/JNEUROSCI.1246-08.2008 [PubMed: 18550763]

Anagnostaras SG, Gale GD, Fanselow MS, 2001 Hippocampus and contextual fear conditioning: Recent controversies and advances. Hippocampus 11, 8–17. https://doi.org/AID-HIPO1015>3.0.CO;2-7 [PubMed: 11261775]

Andreatta M, Glotzbach-Schoon E, Mühlberger A, Schulz SM, Wiemer J, Pauli P, 2015 Initial and sustained brain responses to contextual conditioned anxiety in humans. Cortex 63, 352–363. 10.1016/j.cortex.2014.09.014 [PubMed: 25460498]

Baeuchl C, Meyer P, Hoppstädter M, Diener C, Flor H, 2015 Contextual fear conditioning in humans using feature-identical contexts. Neurobiol. Learn. Mem 121, 1–11. 10.1016/j.nlm.2015.03.001 [PubMed: 25792231]

Baumann O, Mattingley JB, 2014 Dissociable roles of the hippocampus and parietal cortex in processing of coordinate and categorical spatial information. Front. Hum. Neurosci 8:73 10.3389/fnhum.2014.00073 [PubMed: 24596551]

Beckmann CF, Smith SM, 2004 Probabilistic independent component analysis for functional magnetic resonance imaging. IEEE Trans. Med. Imaging 23, 137–152. 10.1109/TMI.2003.822821 [PubMed: 14964560]

Benjamini Y, Hochberg Y, 1995 Controlling the False Discovery Rate: A Practical and Powerful Approach to Multiple Testing. J. R. Stat. Soc. Ser. B 57, 289–300.

Boucsein W, Fowles DC, Grimnes S, Ben-Shakhar G, roth WT, Dawson ME, Filion DL, 2012 Publication recommendations for electrodermal measurements. Psychophysiology 49, 1017–1034. 10.1111/j.1469-8986.2012.01384.x [PubMed: 22680988]

Brinkmann L, Poller H, Herrmann MJ, Miltner W, Straube T, 2017 Initial and sustained brain responses to threat anticipation in blood-injection-injury phobia. NeuroImage Clin. 13, 320–329. 10.1016/j.nicl.2016.12.015 [PubMed: 28066706]

Brodt S, Pöhlchen D, Flanagin VL, Glasauer S, Gais S, Schönauer M, 2016 Rapid and independent memory formation in the parietal cortex. Proc. Natl. Acad. Sci 113, 13251–LP13256. [PubMed: 27803331]

Cabeza R, Ciaramelli E, Olson IR, Moscovitch M, 2008 The parietal cortex and episodic memory: An attentional account. Nat. Rev. Neurosci 9, 613–625. 10.1038/nrn2459 [PubMed: 18641668]

Chen G, Saad ZS, Britton JC, Pine DS, Cox RW, 2013 Linear mixed-effects modeling approach to FMRI group analysis. Neuroimage 73, 176–190. 10.1016/j.neuroimage.2013.01.047 [PubMed: 23376789]

Corcoran KA, Maren S, 2001 Hippocampal Inactivation Disrupts Contextual Retrieval of Fear Memory after Extinction. J. Neurosci 21, 1720. [PubMed: 11222661]

Cox RW, 1996 AFNI: Software for Analysis and Visualization of Functional Magnetic Resonance Neuroimages. Comput. Biomed. Res 29, 162–173.

Cox RW, Chen G, Glen DR, Reynolds RC, Taylor PA, 2017 FMRI Clustering in AFNI: False-Positive Rates Redux. Brain Connect. 7, 152–171. 10.1089/brain.2016.0475 [PubMed: 28398812]

Craig AD, 2009 How do you feel - now? The anterior insula and human awareness. Nat. Rev. Neurosci 10, 59–70. 10.1038/nrn2555 [PubMed: 19096369]

Drabant EM, Kuo JR, Ramel W, Blechert J, Edge MD, Cooper JR, Goldin PR, Hariri AR, Gross JJ, 2011 Experiential, autonomic, and neural responses during threat anticipation vary as a function of threat intensity and neuroticism. Neuroimage 55, 401–410. 10.1016/j.neuroimage.2010.11.040 [PubMed: 21093595]

Fang P-C, Stepniewska I, Kaas JH, 2006 The thalamic connections of motor, premotor, and prefrontal areas of cortex in a prosimian primate (Otolemur garnetti). Neuroscience 143, 987–1020. 10.1016/j.neuroscience.2006.08.053 [PubMed: 17055664]

Fanselow MS, 2000 Contextual fear, gestalt memories, and the hippocampus. Behav. Brain Res 110, 73–81. 10.1016/S0166-4328(99)00186-2 [PubMed: 10802305]

Fullana MA, Harrison BJ, Soriano-Mas C, Vervliet B, Cardoner N, Àvila-Parcet A, Radua J, 2016 Neural signatures of human fear conditioning: An updated and extended meta-analysis of fMRI studies. Mol. Psychiatry 21, 500–508. 10.1038/mp.2015.88 [PubMed: 26122585]

Glenn DE, Risbrough VB, Simmons AN, Acheson DT, Stout DM, 2018 The future of contextual fear learning for PTSD research: A methodological review of neuroimaging studies. Curr. Top. Behav. Neurosci 38, 207–228. 10.1007/7854_2017_30 [PubMed: 29063483]

Glotzbach-Schoon E, Andreatta M, Mühlberger A, Pauli P, 2013 Context conditioning in virtual reality as a model for pathological anxiety. e-Neuroforum 19:63 10.1007/s13295-013-0047-z

Grupe DW, Nitschke JB, 2013 Uncertainty and anticipation in anxiety: An integrated neurobiological and psychological perspective. Nat. Rev. Neurosci 14, 488–501. [PubMed: 23783199]

Grupe DW, Oathes DJ, Nitschke JB, 2013 Dissecting the anticipation of aversion reveals dissociable neural networks. Cereb. Cortex 23, 1874–1883. 10.1093/cercor/bhs175 [PubMed: 22763169]

Joshi SA, Duval ER, Kubat B, Liberzon I, 2019 A review of hippocampal activation in post-traumatic stress disorder. Psychophysiology 0, e13357 10.1111/psyp.13357

Kaufamn L, Rousseeuw PJ, 2008 Finding Groups in Data: An Introduction to Clustering Analysis. John Wiley & Sons, Inc., Hoboken, New Jersey.

Kelly RE, Alexopoulos GS, Wang Z, Gunning FM, Murphy CF, Morimoto SS, Kanellopoulos D, Jia Z, Lim KO, Hoptman MJ, 2010 Visual inspection of independent components: Defining a procedure for artifact removal from fMRI data. J. Neurosci. Methods 189, 233–245. [PubMed: 20381530]

Khalsa SS, Rudrauf D, Feinstein JS, Tranel D, 2009 The pathways of interoceptive awareness. Nat. Neurosci 12, 1494–1496. 10.1038/nn.2411 [PubMed: 19881506]

Kheirbek MA, Drew LJ, Burghardt NS, Costantini DO, Tannenholz L, Ahmari SE, Zeng H, Fenton AA, Hen R, 2013 Differential Control of Learning and Anxiety along the Dorsoventral Axis of the Dentate Gyrus. Neuron 77, 955–968. 10.1016/j.neuron.2012.12.038 [PubMed: 23473324]

Knapska E, Macias M, Mikosz M, Nowak A, Owczarek D, Wawrzyniak M, Pieprzyk M, Cymerman IA, Werka T, Sheng M, Maren S, Jaworski J, Kaczmarek L, 2012 Functional anatomy of neural circuits regulating fear and extinction. Proc. Natl. Acad. Sci 109, 17093–17098. 10.1073/pnas.1202087109 [PubMed: 23027931]

Lang S, Kroll A, Lipinski SJ, Wessa M, Ridder S, Christmann C, Schad LR, Flor H, 2009 Context conditioning and extinction in humans: Differential contribution of the hippocampus, amygdala and prefrontal cortex. Eur. J. Neurosci 29, 823–832. 10.1111/j.1460-9568.2009.06624.x [PubMed: 19200075]

Ledoux J, Daw ND, 2018 Surviving threats: Neural circuit and computational implications of a new taxonomy of defensive behaviour. Nat. Rev. Neurosci 19, 269–282. 10.1038/nrn.2018.22 [PubMed: 29593300]

Liberzon I, Abelson JL, 2016 Context Processing and the Neurobiology of Post-Traumatic Stress Disorder. Neuron 92, 13–30. 10.1016/j.neuron.2016.09.039

Lonsdorf TB, Menz MM, Andreatta M, Fullana MA, Golkar A, Haaker J, Heitland I, Hermann A, Kuhn M, Kruse O, Meir Drexler S, Meulders A, Nees F, Pittig A, Richter J, Romer S, Shiban Y, Schmitz A, Straube B, Vervliet B, Wendt J, Baas JMP, Merz CJ, 2017 Don't fear "fear conditioning": Methodological considerations for the design and analysis of studies on human fear acquisition, extinction, and return of fear. Neurosci. Biobehav. Rev 77, 247–285. 10.1016/j.neubiorev.2017.02.026 [PubMed: 28263758]

Lonsdorf TB, Merz CJ, 2017 More than just noise: Inter-individual differences in fear acquisition, extinction and return of fear in humans - Biological, experiential, temperamental factors, and methodological pitfalls. Neurosci. Biobehav. Rev 80, 703–728. 10.1016/j.neubiorev.2017.07.007 [PubMed: 28764976]

Maddox SA, Hartmann J, Ross RA, Ressler KJ, 2019 Deconstructing the Gestalt: Mechanisms of Fear, Threat, and Trauma Memory Encoding. Neuron 102, 60–74. 10.1016/j.neuron.2019.03.017 [PubMed: 30946827]

Makoshi Z, Kroliczak G, Van Donkelaar P, 2011 Human supplementary motor area contribution to predictive motor planning. J. Mot. Behav 43, 303–309. 10.1080/00222895.2011.584085 [PubMed: 21732868]

Maren S, Phan KL, Liberzon I, 2013 The contextual brain: Implications for fear conditioning, extinction and psychopathology. Nat. Rev. Neurosci 14, 417–428. 10.1038/nrn3492 [PubMed: 23635870]

Marschner A, Kalisch R, Vervliet B, Vansteenwegen D, Buchel C, 2008 Dissociable Roles for the Hippocampus and the Amygdala in Human Cued versus Context Fear Conditioning. J. Neurosci 28, 9030–9036. 10.1523/JNEUROSCI.1651-08.2008 [PubMed: 18768697]

Monti JM, Cooke GE, Watson PD, Voss MW, Kramer AF, Cohen NJ, 2014 Relating Hippocampus to Relational Memory Processing across Domains and Delays. J. Cogn. Neurosci 27, 234–245. 10.1162/jocn_a_00717

O'Muircheartaigh J, Keller SS, Barker GJ, Richardson MP, 2015 White Matter Connectivity of the Thalamus Delineates the Functional Architecture of Competing Thalamocortical Systems. Cereb. Cortex 25, 4477–4489. 10.1093/cercor/bhv063 [PubMed: 25899706]

Orr SP, Metzger LJ, Lasko NB, Macklin ML, Peri T, Pitman RK, 2000 De novo conditioning in trauma-exposed individuals with and without posttraumatic stress disorder. J. Abnorm. Psychol 109, 290–298. [PubMed: 10895567]

Pedersen WS, Balderston NL, Miskovich TA, Belleau EL, Helmstetter FJ, Larson CL, 2017a The effects of stimulus novelty and negativity on BOLD activity in the amygdala, hippocampus, and bed nucleus of the stria terminalis. Soc. Cogn. Affect. Neurosci 12, 748–757. 10.1093/scan/nsw178 [PubMed: 28008079]

Pedersen WS, Muftuler LT, Larson CL, 2017b Disentangling the effects of novelty, valence and trait anxiety in the bed nucleus of the stria terminalis, amygdala and hippocampus with high resolution 7T fMRI. Neuroimage 156, 293–301. 10.1016/j.neuroimage.2017.05.009 [PubMed: 28502843]

Pineles SL, Nillni YI, King MW, Patton SC, Bauer MR, Mostoufi SM, Gerber MR, Hauger R, Resick PA, Rasmusson AM, Orr SP, 2016 Extinction retention and the menstrual cycle: Different associations for women with Posttraumatic Stress Disorder. J. Abnorm. Psychol 125, 349–355. [PubMed: 26866677]

Pineles SL, Orr MR, Orr SP, 2009 An alternative scoring method for skin conductance responding in a differential fear conditioning paradigm with a long-duration conditioned stimulus. Psychophysiology 46, 984–995. 10.1111/j.1469-8986.2009.00852.x [PubMed: 19558401]

Pohlack ST, Nees F, Ruttorf M, Schad LR, Flor H, 2012 Activation of the ventral striatum during aversive contextual conditioning in humans. Biol. Psychol 91, 74–80. 10.1016/j.biopsycho.2012.04.004 [PubMed: 22560888]

Rikhye RV, Gilra A, Halassa MM, 2018 Thalamic regulation of switching between cortical representations enables cognitive flexibility. Nat. Neurosci 21, 1753–1763. 10.1038/s41593-018-0269-z [PubMed: 30455456]

Robin J, Hirshhorn M, Rosenbaum RS, Winocur G, Moscovitch M, Grady CL, 2015 Functional connectivity of hippocampal and prefrontal networks during episodic and spatial memory based on real-world environments. Hippocampus 25, 81–93. 10.1002/hipo.22352 [PubMed: 25154600]

Rudy JW, 2009 Context representations, context functions, and the parahippocampal–hippocampal system. Learn. Mem 16, 573–585. 10.1101/lm.1494409 [PubMed: 19794181]

Rudy JW, Huff NC, Matus-Amat P, 2004 Understanding contextual fear conditioning: insights from a two-process model. Neurosci. Biobehav. Rev 28, 675–685. [PubMed: 15555677]

Saj A, Verdon V, Hauert C-A, Vuilleumier P, 2018 Dissociable components of spatial neglect associated with frontal and parietal lesions. Neuropsychologia 115, 60–69. [PubMed: 29477838]

Segerdahl AR, Mezue M, Okell TW, Farrar JT, Tracey I, 2015 The dorsal posterior insula subserves a fundamental role in human pain. Nat. Neurosci 18, 499–500. 10.1038/nn.3969 [PubMed: 25751532]

Somerville LH, Wagner DD, Wig GS, Moran JM, Whalen PJ, Kelley WM, 2013 Interactions between transient and sustained neural signals support the generation and regulation of anxious emotion. Cereb. Cortex 23, 49–60. 10.1093/cercor/bhr373 [PubMed: 22250290]

Steiger F, Nees F, Wicking M, Lang S, Flor H, 2015 Behavioral and central correlates of contextual fear learning and contextual modulation of cued fear in posttraumatic stress disorder. Int. J. Psychophysiol 98, 584–593. 10.1016/j.ijpsycho.2015.06.009 [PubMed: 26149734]

Stout DM, Glenn DE, Acheson DT, Spadoni AD, Risbrough VB, Simmons AN, 2018 Neural measures associated with configural threat acquisition. Neurobiol. Learn. Mem 150, 99–106. 10.1016/j.nlm.2018.03.012 [PubMed: 29544725]

Tibshirani R, Walther G, Hastie T, 2002 Estimating the number of clusters in a data set via the gap statistic. J. R. Stat. Soc. Ser. B 63, 411–423. 10.1111/1467-9868.00293

Urcelay GP, Miller RR, 2014 The functions of contexts in associative learning. Behav. Processes 104, 2–12. 10.1016/j.beproc.2014.02.008 [PubMed: 24614400]

Vogt AB, 2005 Pain and emotion interactions in subregions of the cingulate gyrus. Nat. Rev. Neurosci 6, 533. [PubMed: 15995724]

Wilcox RR, Keselman HJ, 2003 Modern Robust Data Analysis Methods: Measures of Central Tendency. Psychol. Methods 8, 254–274. 10.1037/1082-989X.8.3.254 [PubMed: 14596490]

Zheng J, Stevenson RF, Mander BA, Mnatsakanyan L, Hsu FPK, Vadera S, Knight RT, Yassa MA, Lin JJ, 2019 Multiplexing of Theta and Alpha Rhythms in the Amygdala-Hippocampal Circuit Supports Pattern Separation of Emotional Information. Neuron. 10.1016/j.neuron.2019.03.025

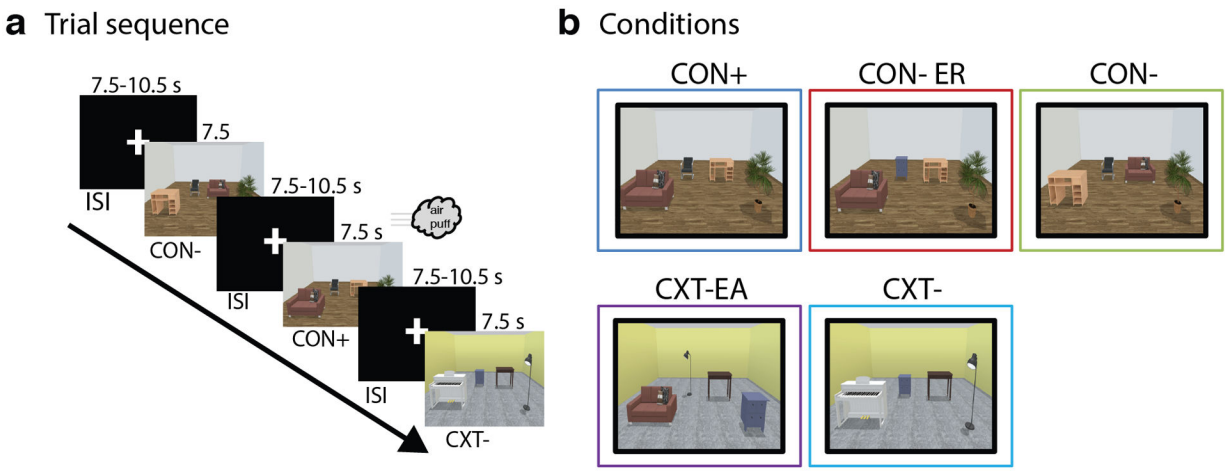

Figure 1.

Configural threat task. (a) Trial sequence and timing for the configural threat learning task. Configurations and contexts were presented for 7.5 s, followed by a 7.5–10.5s ITI. The US co-terminated with the CON+ on 100% of trials. No other conditions co-terminated with a US. (b) Examples for the five conditions. CON+, CON-ER, and CON- were configural learning trials and had the same background but with different arrangements of the same furniture. CXT-EA and CXT- were configural learning conditions with different furniture in a different room (see Method section and Table 1 section for more details).

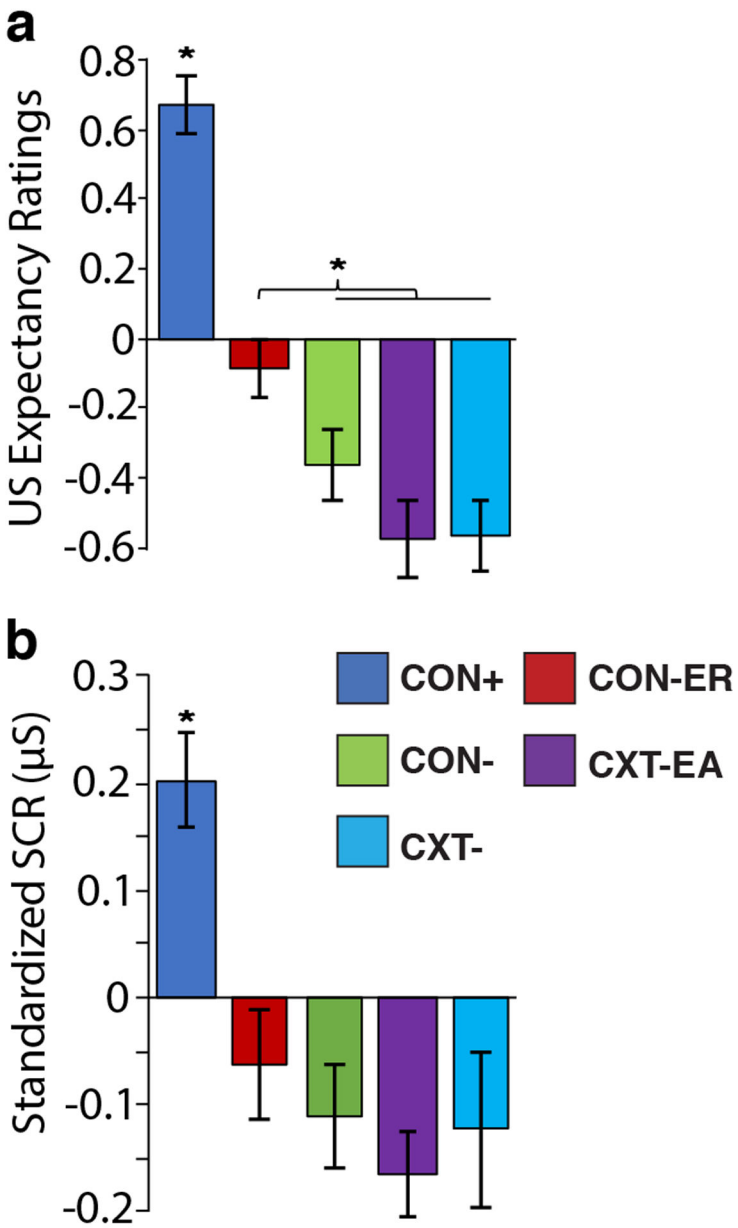

Figure 2.

SCR and US expectancy ratings. (a) Bar plots depicting the significant main effect of CS Type for US expectancy ratings. (b) Bar plot depicts the significant CS Type main effect for SCR. SCR is plotted as the standardized (within-subject *Z*-score) in μS. Error bars depict standard error of the mean (S.E.M.). *= $q<.05$ (FDR corrected).

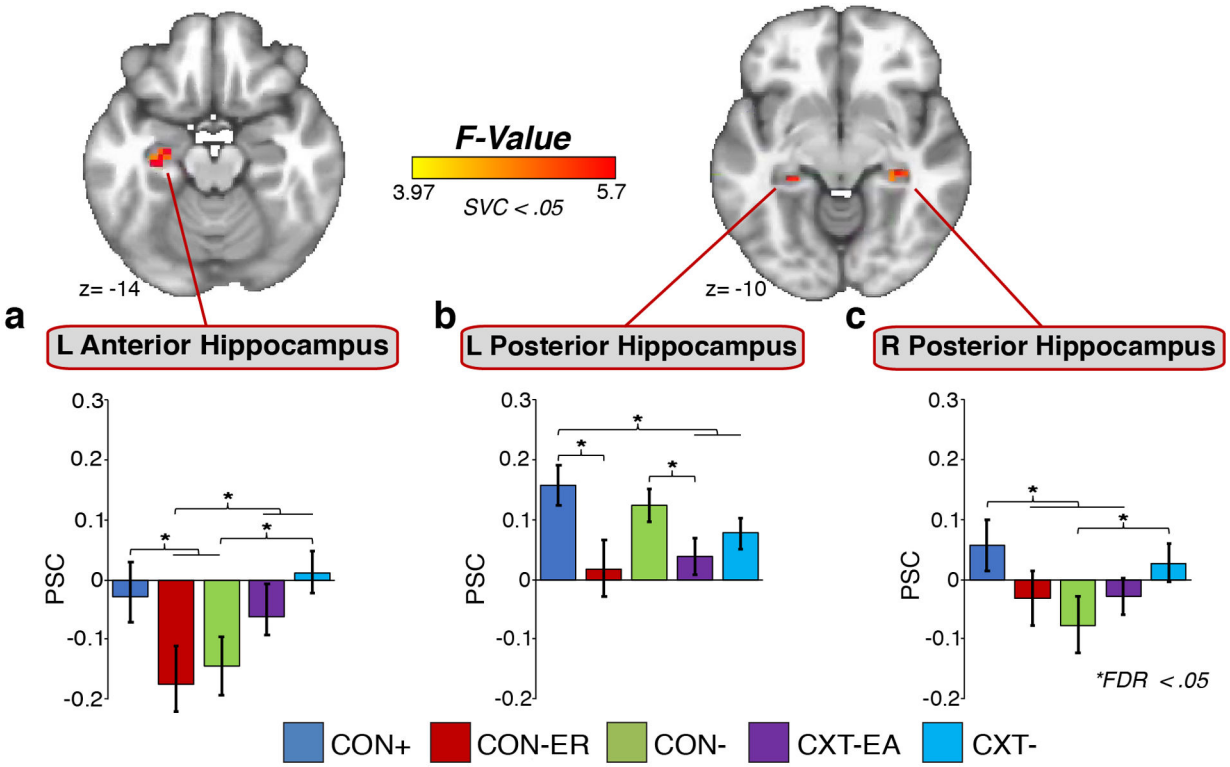

Figure 3.

Results for the hippocampus region of interest analysis (ROI). Significant effects were identified in three regions within the hippocampus (panels a-c). The left and right hippocampus ROIs were created from the Harvard-Oxford probabilistic atlas. These analyses were thresholded (p<.005) and small volume corrected (SVC; α < .05). Error bars depict standard error of the mean (S.E.M.). *= q<.05 (FDR corrected).

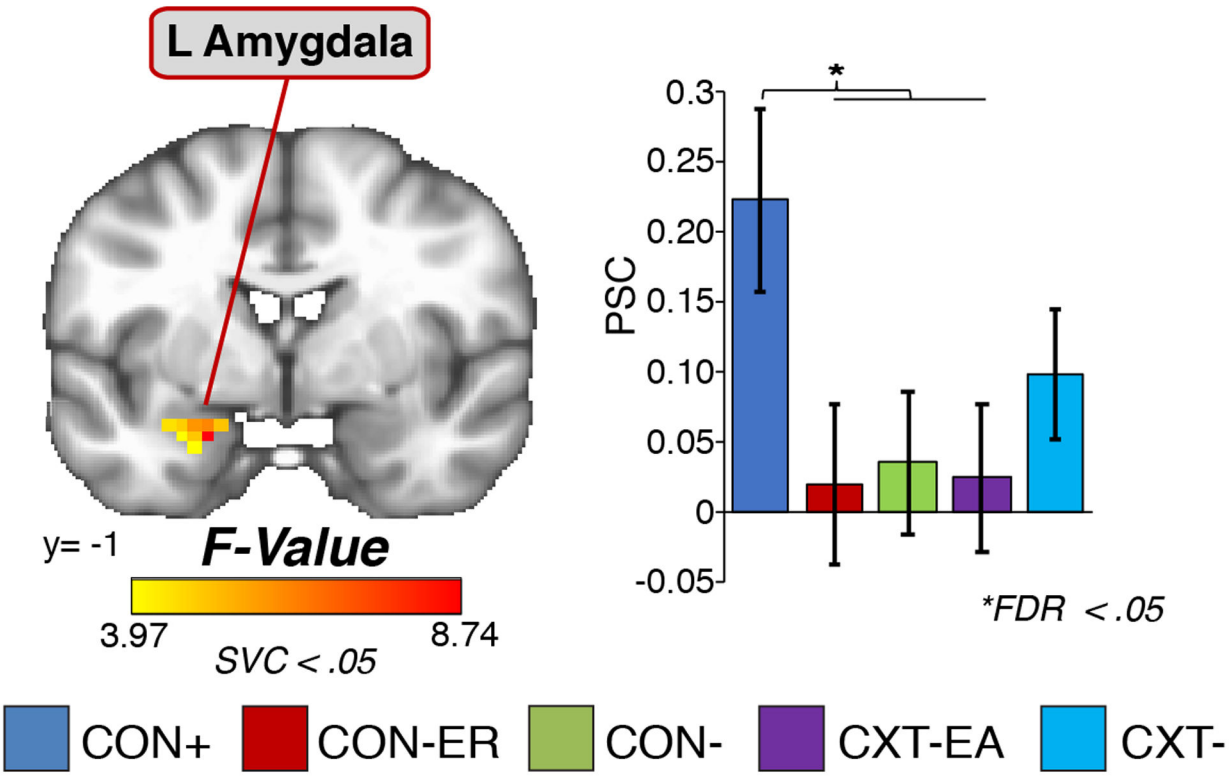

Figure 4.

Results for the amygdala region of interest analysis (ROI). Significant effects were observed in the left amygdala. The amygdala ROI was created using a bilateral mask using the Harvard-Oxford probabilistic atlas. These analyses were thresholded (p<.005) and small volume corrected (SVC; $\alpha < .05$). Error bars depict standard error of the mean (S.E.M.). *= q<.05 (FDR corrected).

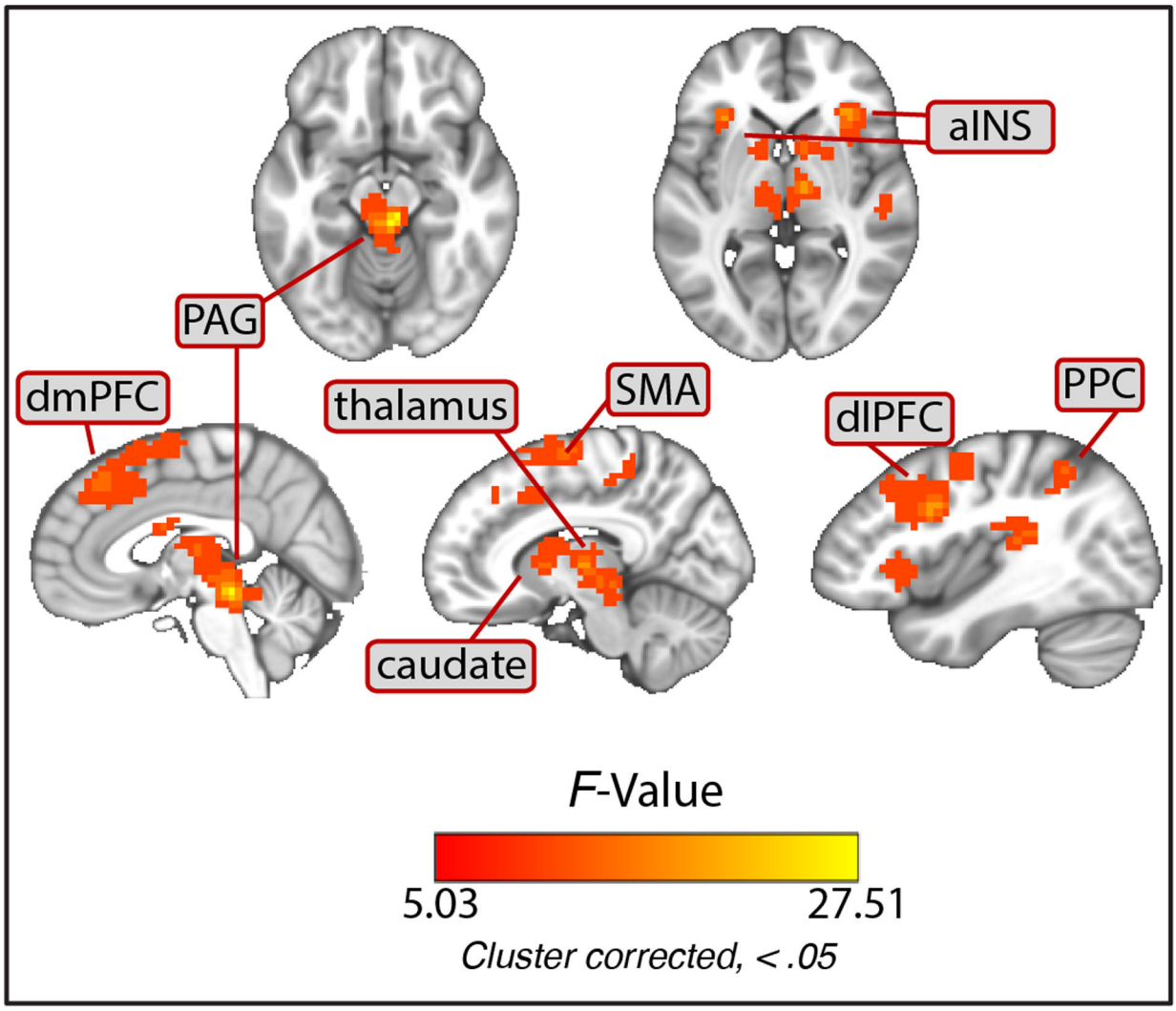

Figure 5.

Results for the whole-brain CS Type linear mixed effects analysis. Significant effects were identified in several regions. Results were voxel-level thresholded (p<.001) and cluster corrected for multiple comparisons (α<.05; cluster-size > 20 voxels).

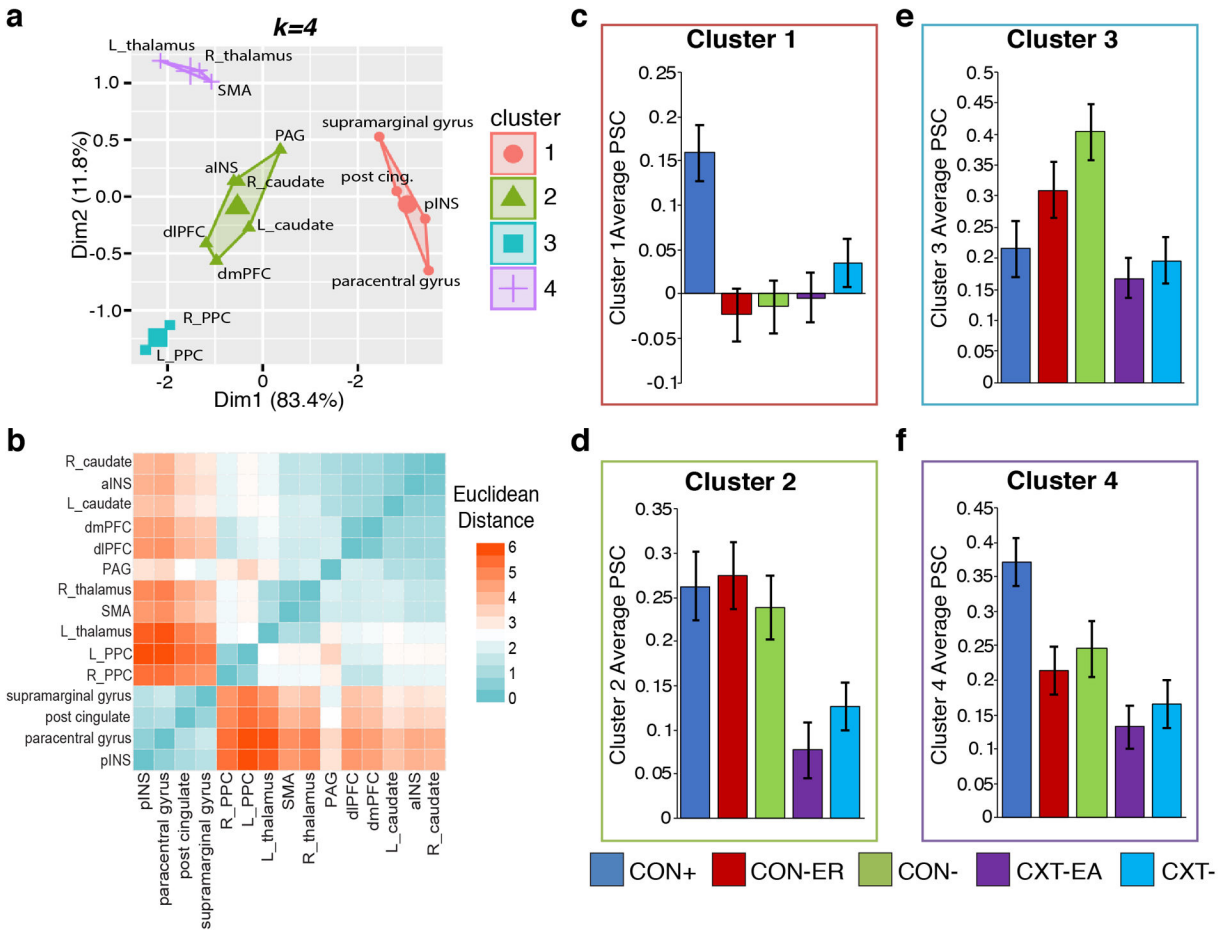

Figure 6.

k-means clustering analysis results. (a) Visual depiction of the *k*=4 clustering results. Data points are plotted as a function of the first two principal components that explain the majority of the variance. (b) Heat map depicting the visualization of the Euclidean distance of each region. Cold colors (blue) depict low distance. (c-f) Bar plots of Clusters 1 through 4 which comprise the average of the regions within each cluster. Error bars depict S.E.M.

Table 1.

Description of task conditions targeting configural encoding

Condition	Configural Demand	US Delivered	Room	Manipulation
CON+		Y	A	Elements in specific arrangement with US delivered
CON-ER	++	N	A	Same elements and arrangement as CON+ but one item replaced
CON-	+++	N	A	Same elements but rearranged
CXT-EA	+	N	B	New elements, but one element added from CON+
CXT-	-	N	B	All new elements

Note. Configural demand column reflects the hypothesized amount of configural encoding demands required to differentiate the condition from the CON+ condition. -None. +Minimal. ++Moderate. +++High.

Table 2.

Whole-brain linear mixed effect results

Region	*X*	*Y*	*Z*	Voxels	*F*-Value	CON+ PSC	CON-ER PSC	CON-PSC	CXT-ER PSC	*CXT-PSC*
PAG	3	−32	−10	285	27.59	.274	.183	.163	.067	.086
R thalamus	10	−12	4	147	15.36	.370	.226	.241	.117	.153
L thalamus	−7	−25	0	125	11.36	.393	.226	.279	.156	.190
R caudate	9	10	5	65	9.99	.278	.279	.213	.078	.124
L caudate	−11	0	11	44	7.80	.242	.264	.225	.063	.132
R SMA	10	−8	67	176	13.02	.352	.191	.216	.122	.148
R paracentral gyrus	24	−29	62	92	9.25	.101	−.057	−.023	−.003	.028
R dmPFC	7	34	46	153	11.41	.241	.306	.301	.091	.143
R dlPFC	42	10	32	318	15.41	.257	.324	.302	.096	.149
R posterior insula	42	−32	18	260	12.00	.137	−.037	−.049	.003	.014
R supramarginal gyrus	56	−26	23	236	9.74	.220	.003	.004	.009	.047
L anterior insula	−32	24	4	60	13.80	.282	.290	.227	.071	.131
L posterior cingulate	−14	−22	39	35	9.41	.176	−.001	.009	−.021	.053
R PPC	42	−50	49	34	9.47	.218	.294	.393	.157	.185
L PPC	−46	−57	60	22	8.03	.213	.325	.414	.179	.209

Note. Abbreviations: R=Right; L=Left; dlPFC=dorsolateral prefrontal cortex; SMA=supplementary motor area; dmPFC = dorsomedial prefrontal cortex; PPC=posterior parietal cortex; PAG=periaqueductal gray area. PSC=percent signal change. *F*-value reflects peak *F*-Value within the cluster. Voxel-size=3.5mm^3. Cluster-thresholded, $p<.001$; whole-brain cluster-corrected $\alpha < .05$ ($k>20$ voxels). PSC for each condition reflects the group-level mean.